Hindawi Publishing Corporation
International Journal of Antennas and Propagation
Volume 2015, Article ID 392714, 15 pages
http://dx.doi.org/10.1155/2015/392714

Research Article

Tracking- and Scintillation-Aware Channel Model for GEO Satellite to Land Mobile Terminals at Ku-Band

Ali M. Al-Saegh,[1] A. Sali,[1] J. S. Mandeep,[2] and Alyani Ismail[1]

[1]*Department of Computer and Communication Systems Engineering, Universiti Putra Malaysia (UPM), 43400 Serdang, Selangor, Malaysia*
[2]*Department of Electrical, Electronic and Systems Engineering, Universiti Kebangsaan Malaysia (UKM), 43600 Bangi, Selangor, Malaysia*

Correspondence should be addressed to Ali M. Al-Saegh; ali.alsaegh84@gmail.com

Received 28 March 2014; Accepted 9 July 2014

Academic Editor: Paschalis Sofotasios

Recent advances in satellite to land mobile terminal services and technologies, which utilize high frequencies with directional antennas, have made the design of an appropriate model for land mobile satellite (LMS) channels a necessity. This paper presents LMS channel model at Ku-band with features that enhance accuracy, comprehensiveness, and reliability. The effect of satellite tracking loss at different mobile terminal speeds is considered for directional mobile antenna systems, a reliable tropospheric scintillation model for an LMS scenario at tropical and temperate regions is presented, and finally a new quality indicator module for different modulation and coding schemes is included. The proposed *extended LMS channel (ELMSC)* model is designed based on actual experimental measurements and can be applied to narrow- and wide-band signals at different regions and at different speeds and multichannel states. The proposed model exhibits lower root mean square error (RMSE) and significant performance observation compared with the conventional model in terms of the signal fluctuations, fade depth, signal-to-noise ratio (SNR), and quality indicators accompanied for several transmission schemes.

1. Introduction

The recent applications and services in the broadcasting satellite communication to land mobile terminal have increased the demand for higher data rate and thus higher transmission frequency. Therefore, land mobile satellite (LMS) channel estimation at high frequency has become a necessity to develop efficient adaptive transmission models and techniques as solutions for channel impairments. Considerable interest has been directed recently toward LMS communication at Ku-band [1], which is the main concern of this study, owing to the high number of existing transponders and the large amount of available bandwidth. Nevertheless, Ku-band receivers require a high-gain directional antenna [1]. A new generation of statistical LMS channel models capable of producing time series generative models was initially introduced for lower frequencies, particularly for L and S bands. These models have replaced the ones that solely provide cumulative distribution functions (CDFs), which are insufficient for appropriate investigations [2].

The LMS channel condition at Ku-band depends on mobility impairments and tropospheric scintillation. The latter, which causes rapid fluctuations in satellite signal level, occurs due to the irregularities in radio refractivity as the wave travels along different medium densities in the troposphere [3, 4]. Several researchers [1, 2, 5–10] have created well-designed LMS channel models. The accuracy of the estimated models has increased notably over time through the addition of several features for approaching the real-world environment along with recent LMS technologies and services. This condition has motivated researchers, as well as the authors of this paper, to design more reliable LMS channel models.

However, existing channel models do not consider tropospheric scintillation under nonrainy conditions, which significantly affect the signal performance at Ku-band, particularly at high humidity regions, such as tropical areas [4]. Moreover,

these models do not consider the impairments caused by different vehicle speeds at Ku-band for systems utilizing mobile directional antenna. Therefore, a comprehensive LMS channel modeling that considers these significant impairments is needed to be designed with lower root mean square error (RMSE).

This paper presents a channel model for satellite to land mobile terminals based on actual measured channel conditions. The proposed model is referred to as *extended LMS channel (ELMSC) model*. The term "extended" refers to four new features included in the model design. Firstly, the improvement is based on actual signal measurements to enhance the accuracy and reliability of the previously developed multistate LMS model at Ku-band. Secondly, the impairment attributed to the variable vehicular speeds is modeled concerning the clear line-of-sight (LOS) and shadowing scenarios. Thirdly, an LMS tropospheric scintillation model is developed. Lastly, a quality indicator module is developed and added to the ELMSC model. The model considers tropospheric scintillation and vehicular environments as well as its application to narrow- and wide-band signals worldwide because the LMS environment varies with respect to different regions in the world, particularly in temperate and tropical regions.

The LMS channel characteristics and impairments regarding the mobility and tropospheric scintillation effects are presented in the next section. The experimental setup is enlightened in Section 3 taking into account the mobility impairments for different states accompanied with tropospheric scintillation. The proposed ELMSC model is presented in Section 4. Section 5 provides a discussion of the results obtained from the measurements and proposed model, along with comparisons made concerning the existing models. The conclusion is presented in Section 6.

2. LMS Channel Characterizations and Impairments

Transmission parameters considerably affect the channel characteristics, the amount of signal attenuation, and the quality of service (QoS) of the LMS signal. In particular, the transmitted frequency, bandwidth, and elevation angle exert effects that should be identified by satellite system designers prior to the design process. The amount of signal attenuation is directly proportional to the carrier frequency and inversely proportional to the elevation angle; thus, the signal quality indication metrics, such as the signal-to-noise ratio (SNR) and energy of bit to noise ratio (E_b/N_o), are affected. For signal frequencies below 3 GHz, ionospheric scintillation has a paramount effect on signal performance. This effect begins to disappear as the frequency increases above the said value [11]. The bandwidth effect will be explained in Section 2.1. The mobility impairments and channel states are presented in Sections 2.2 and 2.3, respectively. The tropospheric scintillation effect is discussed in Section 2.4.

2.1. Bandwidth and Directional Antenna. The bandwidth of the signal is considered narrow-band when it is smaller than the coherence bandwidth; otherwise, it is wide-band. The coherence bandwidth, which is inversely proportional to the delay spread, is typically in the range of 7 MHz to 11 MHz at L-band and approximately 30 MHz at EHF band [1, 12]. Under the narrow-band condition, which is the most probable condition in the LMS channel [13], the channel causes signal amplitude variations, whereas the time dispersion (time delay of the received echoes) is insignificant. Under the wide-band condition, the channel not only causes variations in signal amplitude but also experiences significant time dispersion in the received signal. This condition will cause distortion effects, such as frequency selectivity or intersymbol interference; this distortion effect is attributed to the arrival of the signal echoes at the receiver at different excess delays with respect to the direct signal [2].

Practically, the radiation pattern of a directional antenna, which is commonly used in LMS scenarios at Ku-band, filters out the echoes with significant delays; therefore, narrow-band models are typically employed for Ku-band signals for narrow- and wide-band signals [1, 12, 14].

2.2. Mobility. Advanced technologies for satellite communication services have resulted in a significant increase in mobile satellite terminals. This condition gave rise to the demand for the estimation of the mobility effect on the satellite link channel. Mobility impairments are typically produced by the shadowing or blockage of signal energy, multipath, and antenna tracking error. Shadowing is usually caused by roadside trees, whereas blockage is normally caused by surrounding tall buildings or bridges. The multipath effect, which can be modeled by Rayleigh distribution [15], is primarily attributed to nearby buildings in urban areas or mountains.

These major factors affect the performance and quality of the received signal and have motivated LMS system designers to build well-formulated mobility channel models to predict the signal performance of mobile scenarios. For accurate modeling, the model design should be based on actual channel condition measurements. Thus, a number of experiments are conducted to compare the measured results with that of our estimated model (discussed in Section 3). The received signal strength in a tropical region is measured in consideration of the scenarios of signal quality degradation using a mobile receiver system mounted at the roof of a car. To the best of our knowledge, this is the first experiment conducted to determine the mobility effects on satellite link channel conditions in tropical regions.

2.3. Channel States and Conventional Model. According to the type of impairments encountered during the movements, LMS channel models can be categorized into single-state and multistate models [16, 17]. The single-state model describes the signal level distribution of a specific propagation environment over time, such as clear LOS, direct signal blockage, or shadowing states. Typically, in a single-state LMS channel, the unblocked LOS signal is modeled by Rice distribution. The

Rice factor (K) is defined as the ratio of carrier to multipath normalized average power. Consider

$$K = \frac{a^2}{2\sigma^2}, \quad (1)$$

where a is the amplitude of the direct signal and σ is the standard deviation. If the signal is totally blocked, it is usually represented by Rayleigh distribution.

Meanwhile, several researchers have established single-state channel models that focus on the shadowing condition; they defined this state as a combination of two distributions. The most used models for the LMS scenario are Suzuki and Loo models, which have gained global attention [13]. Loo model assumes that, in the case of shadowing, the Rician-distributed direct signal amplitude varies according to a log-normal distribution, and the received complex envelope consists of the sum of the two phasors. The model considers the change in the phase caused by the Doppler effect, which is practically detected by the omnidirectional antenna. Loo model is applied to multistate LMS channel models at L and S bands [10, 16, 18]. Suzuki model is a combination of Rayleigh and log-normal distributions and is conventionally applied to the modeling of multistate LMS channels at Ku-band using directional antenna [1].

However, in a real-world environment, two or more LMS channel states may occur during normal satellite terminal movement. Therefore, the signal performance exhibits several significant transformations in its characteristics over time unlike the terrestrial scenario whose behavior is usually described by a single distribution [2]. In such case, multistate statistical models should be used to design LMS channel models [2, 19].

Based on data obtained from measurement campaigns in Europe, Lutz et al. [8] designed a two-state model that estimates the LMS signal performance under clear sky (Rician distribution) and signal blockage (Rayleigh distribution) conditions. A high-state channel model is typically based on the Markov chain approach [15, 19]. The Markov chain is a stochastic model in which a system takes on discrete states. This approach is commonly used to model the variations in signal performance attributed to shadowing or blockage effects [10]. The correlation between rain impairment and mobility impairment at Ku-band is presented in [9]; they modified the Rice factor to include the rainy sky scenario.

The first stochastic multistate model based on received signal measurements at Ku-band was supported by the European Space Agency (ESA) [1]. A three-state channel model that reflects the proper approach for the real-world environment, including clear sky, shadowing, and blockage scenarios with multipath effect, was employed. The model was built based on the measurement campaign in Germany with a constant high speed of 120 Km/h in a highway environment and lower than 60 Km/h in other environments. However, the receiver antenna was mounted on a mechanically steerable platform during measurements; this condition may cause pointing misalignments and hence a high tracking accuracy error.

The International Telecommunication Union (ITU) [20] recommended the use of a three-state model for statistical-approach LMS channel modeling. Moreover, [2] stated that the three-state model provides a tradeoff between complexity and accuracy. For the aforementioned reasons, a three-state channel is utilized in the proposed model. Thus, the model is compared with the conventional model [1] that also implemented the three-state scenarios at Ku-band, as explained in the previous paragraph. Nevertheless, other states can be added besides the aforementioned three states; however, this condition represents only special case modeling, such as that presented in [10, 18], where a fourth state was added. The former described the fourth state as signal unavailability attributed to the failure of the satellite tracking process for very low elevation angles (lower than 10°), whereas the fourth state of the latter represented multisatellite diversity (angle diversity).

2.4. Tropospheric Scintillation. Tropospheric scintillation occurs inherently as the wave travels along different medium densities in the troposphere and causes rapid fluctuations in satellite signal level due to irregularities in radio refractivity [3, 21]. The standard deviation of fluctuations in tropical regions differs from that in temperate regions owing to their different related weather parameters, particularly the temperature and humidity of the medium. Accordingly, this condition results in different satellite channel assessments and signal quality performance. However, tropical regions are warmer and have higher relative humidity (H_R) than temperate regions for most time of the year [22]. ITU [23] claimed that the fade depth of tropospheric scintillation may reach a few dBs based on its probability of exceedance time.

3. Experimental Setup

To achieve accurate channel estimation, the model design should be based on the measured values of the LMS channel conditions. Several experiments were therefore conducted to measure the received signal level at the receiver (installed in a vehicle) at different mobility impairments. The impairments that occur typically in everyday life were considered (Figure 1), namely, effects attributed to different vehicle speeds (up to 150 Km/h), shadowing by roadside trees, and blockage by crossroad bridges.

The experimental measurements obtained in the southernmost region of Kuala Lumpur in Malaysia are shown in Figure 2. The measurements are represented by the three states listed in Table 1.

A mobile antenna system (upper right image of Figure 2) was used in the measurements setup mounted at the roof of a car (upper left image of Figure 2). The system consists of a 0.44 m mobile autosteerable antenna pointed at MEASAT 3/3A broadcasting satellite (91.5°E) at 76.5° elevation angle. A high tracking rate (75°/sec) antenna was employed to reduce the tracking error as much as possible. The antenna system also includes a built-in motor and gyroscope to point to the satellite automatically. The detection, filtering, and amplification processes were performed by the antenna system

Table 1: Measurements scenarios.

State number	Scenario	Details
State 1	Clear sky/different speeds	The vehicle moved at different speeds (from 0 km/h up to 150 km/h) during clear LOS. Measurements at zero speed (stationary) were obtained as well.
State 2	Shadowing	The vehicle moved at constant speed (40 km/h) under link shadowing by tall trees (approximately 12 m tall and 7 m away from the vehicle on the average) on the roadsides.
State 3	Blockage	The vehicle moved at constant speed (40 km/h) under blockage by road bridges.

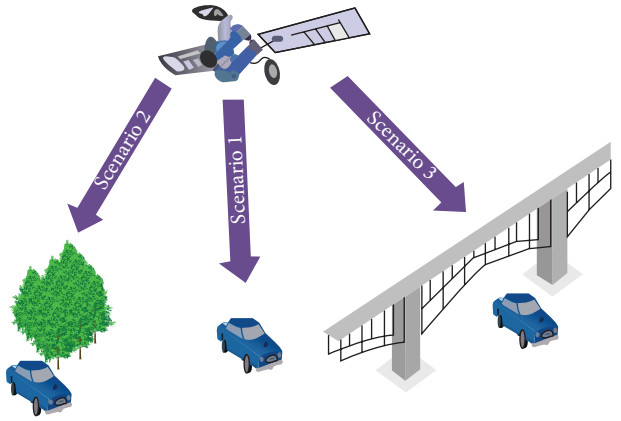

Figure 1: LMS link scenarios.

Figure 2: Measurements campaign.

before the down conversion to L-band IF by a 9.75 GHz local oscillator.

As the signals pass through the mobile antenna system, they are split into two directions as shown in Figure 3; the first direction is toward the decoder, and the second is toward the spectrum analyzer for data evaluation and analysis.

Meanwhile, the relative humidity was obtained on the day of the measurement campaign from the Malaysian Meteorological Department (MMD). The satellite and receiver systems parameters are listed in Table 2.

Typically, when the directional antenna is used, the reflections from buildings come from angles that are different from those in the satellite direction. This condition causes

Table 2: LMS system parameters.

EIRP	57 dBW
Antenna elevation angle	76.5°
Polarization	Horizontal
Antenna local oscillator	9.75 GHz
Radio frequency (RF)	11.68 GHz
Intermediate frequency (IF)	1.93 GHz
Antenna diameter	0.44 m
Antenna tracking rate	75°/s

Table 3: Channel states probabilities.

Probability	Value
P_1	$\frac{836}{875} = 0.955$
P_2	$\frac{21}{875} = 0.024$
P_3	$\frac{18}{875} = 0.021$

the reflections from the buildings to be rarely measured [1]. The measurement campaign was conducted in highway and suburban areas as shown in Figure 2. The areas contain many crossroad bridges, tunnels, and road toll counters (whose sheds cause signal blockages) as well as roadside trees that cause shadowing because of their dense leaves and branches. During the continuous measurements, 837 data recordings were obtained at a clear sky state at various vehicle speeds, whereas 21 and 17 recordings were obtained during signal shadowing and blockage, respectively. The probability of accordance of each state is obtained depending on the aforementioned numbers of recordings and shown in Table 3.

The large number of measured samples is used in the comparison with the measured data to improve the accuracy of the ELMSC model. However, the probability of each state can be assumed in the design of the LMS channel model according to the environment of the specified region of interest.

4. ELMSC Model

Fading channel model and characterization gain the outmost importance for systems utilizing LMS link adaptive techniques and channel-aware modeling performance evaluation and assessment. The proposed model consists of several sections as shown in Figure 4. These sections include the

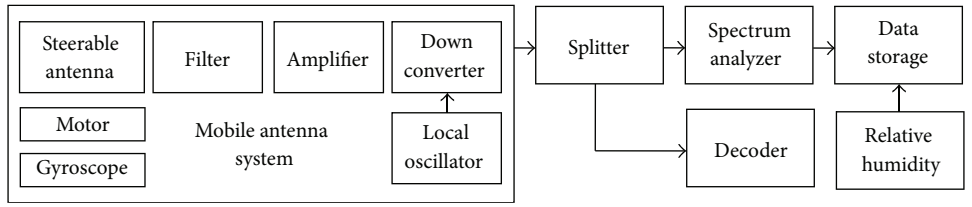

Figure 3: Measurement setup.

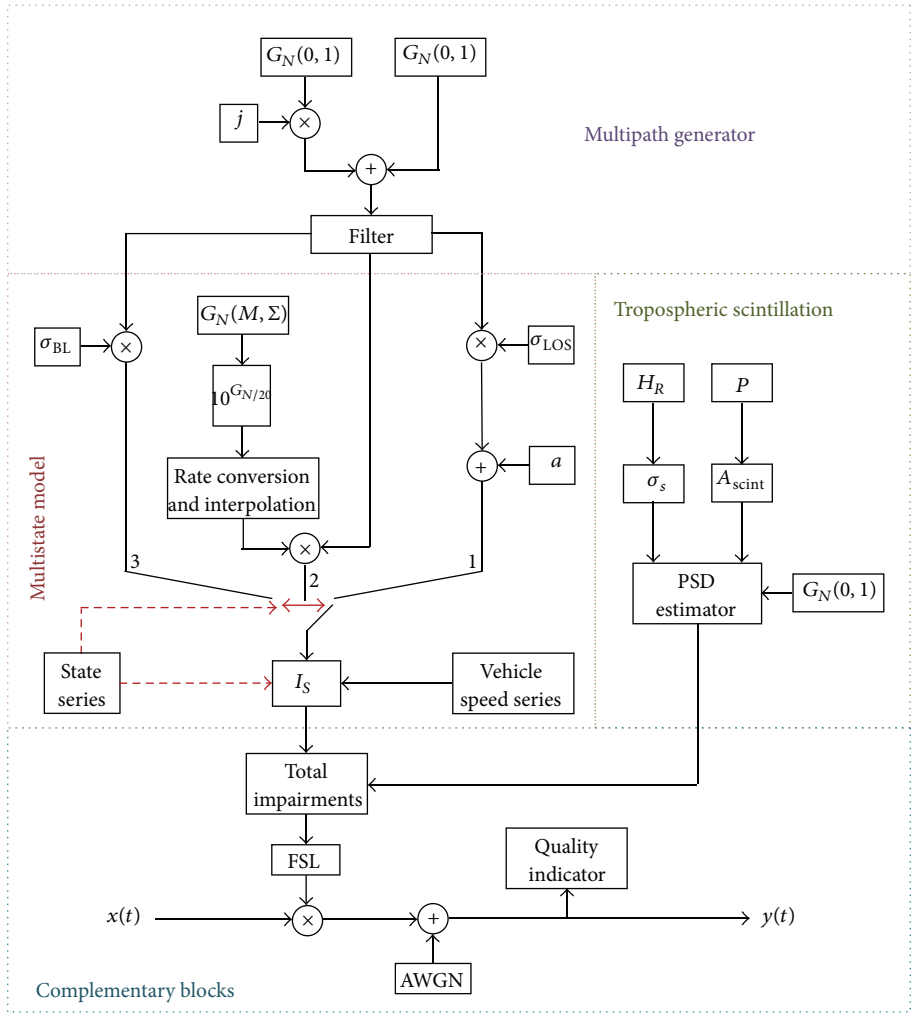

Figure 4: Proposed ELMSC model.

multipath generation, the multistate model, the tropospheric scintillation model, the complementary blocks, and the quality indicator module. The model is designed based on the actual experimental measurements presented in Section 3.

In an actual LMS environment, channel output $y(t)$ can be defined as

$$y(t) = x(t) f(t) + n(t), \tag{2}$$

where $x(t)$ is the transmitted signal, $f(t)$ is the LMS channel fading, and $n(t)$ is the signal noise. The proposed ELMSC model imposes a comprehensive impairments estimation effect which includes the impairments of mobility $m(t)$ and tropospheric scintillation $s(t)$. Consider

$$f_m(t) = m(t) s(t), \tag{3}$$

where $f_m(t)$ is the total mobility impairments. The mobility impairments of the LMS channel include the attenuation attributed to the satellite terminal speed, shadowing or blockage attributed to physical obstacles in the link, and the multipath effect. In practice, both impairments are modeled separately to produce the time series for correlated scintillation and mobility impairments. Afterwards, their values are correlated according to the mobility state environment. The

details of the proposed model blocks are explained in the subsequent subsections.

4.1. Multipath Generator. The diffused multipath fading model can be characterized by Rayleigh distribution [15]. The envelope is a result of the reflected signals from number of paths N as illustrated in (4). Consider

$$r(t) = \sum_{i=1}^{N} A_i(t) \exp\left[j\,\Gamma_i(t)\right], \tag{4}$$

where $A_i(t)$ is the reflected power of the ith signals and $\Gamma_i(t)$ is a coefficient that depends on angular Doppler frequency ω_D as well as angle of arrival β and phase ϕ as expressed in (5). Consider

$$\Gamma_i(t) = \omega_D \cos\beta_i(t) + \phi(t). \tag{5}$$

Therefore, (4) can be rewritten as (6) or (7). Consider

$$r(t) = A(t) \sum_{i}^{N} \cos\Gamma_i(t) + jA(t) \sum_{i}^{N} \sin\Gamma_i(t), \tag{6}$$

$$r(t) = r_I(t) + jr_Q(t), \tag{7}$$

where $r_I(t)$ and $r_Q(t)$ represent the inphase and quadrature components of the Rayleigh distribution, respectively. These two components, as predicted by the central limit theorem, can be produced by first generating two, zero-mean white Gaussian distributions [13, 24] as shown in Figure 4. The standard deviation σ varies with respect to the clear sky, shadowing, and blockage states because the fluctuation level attributed to the multipath effect differs with respect to each state [13]. σ reaches the maximum in the blockage state and minimum in the state of clear LOS. Therefore, σ is included in the multistate model (explained in Section 4.2).

Power spectral shaping is achieved by coloring "filtering" the resultant complex signal. The inphase and quadrature trails are filtered with a Doppler filter to shape "reproduce" the Doppler effects for the fading channel attributed to the motion of the terminal. The filtering process is necessary in simulating the channel. Without this process, the resultant signal variations would be unnaturally fast for a given satellite terminal speed and would thus produce error bursts and distribution of outage durations [25]. Therefore, a Butterworth filter is used in the proposed model; this filter is commonly used in LMS channel modeling because it provides a more realistic approach [13, 24, 26, 27]. The filtering process is designed based on [13, 27].

4.2. Multistate Model. Three states, namely, clear LOS, shadowing, and blockage states, were implemented in the ELMSC model. The model introduces one of the extensions of the ELMSC model that represents the losses of satellite terminal attributed to movements at different speeds (I_S); the new extension is applied to the clear LOS and shadowing states.

The cumulative distribution of the resultant signal should be the weighted combination of the three states [10, 23]. Therefore, the probability behavior for the three states is expressed in (8). Consider

$$P(n \le N) = P_1 m_1 + P_2 m_2 + P_3 m, \tag{8}$$

where n is the sample number from the total number of samples N. P_i is the probability of occurrence of the ith state ($P_1 + P_2 + P_3 = 1$). The probabilities were obtained from the experimental measurements as mentioned in Section 3 and were used to generate random state series. The total time (or number of samples) of being in a specific state depends on the probability of occurrence. The output discrete signal is a result of switching between the generated signal samples of the aforementioned states according to the state series.

4.2.1. Clear LOS Signal Model. The signal received by the mobile satellite terminal moving at different speeds in a clear (unblocked) channel environment is usually modeled with Rician distribution as discussed in Section 2.3. The model includes the constant direct signal with multipath fluctuations. The latter, Rician multipath, is designed by first multiplying the resultant signal from the multipath model discussed in Section 4.1 with its specific standard deviation (σ_{LOS}). The direct signal component (a) is then added to the Rician multipath signal. a is extracted using (1), where K represents the ratio between the direct signal level and the noise floor level. Therefore, our assumption on the Rice factor is based on the actual measurements of the signal. Typically, the noise floor level is assumed based on the measurement setup [1, 2].

Moreover, to estimate the signal losses that may occur because of the antenna tracking error attributed to terminal movements, a new formula is proposed (see (9)) to estimate the signal losses for satellite terminal movements at different speeds in dB based on the actual measurement explained in Section 3. Consider

$$I_S = k_a s^2 + k_b s + k_c, \tag{9}$$

where s is the satellite terminal speed in km/h and the constant values k_a, k_b, and k_c are -4.667×10^{-5}, 1.468×10^{-2}, and -1.364×10^{-3}, respectively. These values were obtained with nonlinear curve-fitting optimization technique; the proposed formula provides accurate mobility impairment estimation with a RMSE of 0.02407. Terminal speed is used as an input to the module. This input series can be generated using sinusoidal distribution random numbers with a minimum value of 0. The maximum value can be assumed based on the nature of the road of interest and its highest permitted speed. Moreover, the probability of speed values can be obtained through statistical observations.

4.2.2. Shadowed Signal Model. The shadowing (state 2) attributed to roadside trees causes additional attenuation to the received signal and thus results in a slow variation in the direct signal simultaneous with the diffuse multipath components. Typically, the shadowed signal at Ku-band is modeled with the Suzuki model [1]. This model involves the combination of log-normal and Rayleigh distributions.

Normal distribution signal G_N is generated with its specific mean M and standard deviation Σ obtained from [1] in dB before being converted to a log-normal distribution using the relation $10^{G_N/20}$. The resultant signal passes through two stages: rate conversation (to identify the slope of the envelop and number of the added samples based on f_S of the fast multipath fluctuations) and interpolation (adding samples between two different leveled samples corresponding to the rate conversation and then convolution for envelope shaping of the interpolated samples). In summary, these steps were implemented to add an interpolated sloped envelop sample to approach the number of multipath samples and to avoid sharp multipath fluctuations. For periods with no state transitions, this rate is utilized to generate rapid variations with a low sampling period to account for the Doppler spread bandwidth [13].

The multipath fluctuations of this state were generated as discussed in Section 4.1. The resultant combination of the two distributions is then obtained to reflect the performance of the signal in the shadowing environment. The impairments that occur primarily because of the antenna tracking error due to the terminal movements, expressed in (9), affect the shadowed signal as well because the direct signal component still exists despite being shadowed. Therefore, in the case of a partially shadowed environment (state 2), the I_S module is also involved in the simulated shadowed signal.

4.2.3. Blocked Signal Model. LMS signal blockage (state 3) is typically caused by bridges across the highway, sheds of the road tolls counters, tunnels, or tall buildings in urban areas. The received signal power vanishes, and the fade depth can be expressed by the noise floor level below the LOS. The LMS signal blockage model is typically designed with Rayleigh distribution with specific standard deviation σ_{BL} as discussed earlier. Therefore, σ_{BL} is applied to the resultant fluctuated signal from the multipath model discussed in Section 4.1. Considering that the direct signal is totally blocked in this state, the signal would be unaffected by the I_S module. The status of the current state is obtained from state series block as shown in Figure 4 to switch the I_S module on during the clear LOS and shadowing states and off during the blockage state.

4.3. Tropospheric Scintillation Model. Tropospheric scintillation depends on its standard deviation (σ_S) [21, 23]. The modeling of tropospheric scintillation effect begins with the generation of a zero-mean white Gaussian distribution and with standard deviation conventionally set to 1 [23, 28]. However, σ_S depends mainly on the relative humidity and the temperature [23], which is different in tropical regions compared with temperate regions according to their weather parameters. For temperate regions, Cioni et al. [28] assumed that the value of σ_S is 0.066. However, it is declared by [22] that the standard deviation of scintillation in tropical regions is larger than that in temperate regions. Therefore, σ_S is adjusted to 0.117 to increase the accuracy of the estimated scintillation standard deviation. The value of σ_S is estimated based on two steps. First, the H_R value was obtained from the MMD as discussed in Section 3. Second, the mean value is used to estimate σ_S according to (10) [23]. Consider

$$\sigma_S = \sigma_0 \, f^{0.583} \frac{g}{(\sin\theta)^{1.2}}, \tag{10}$$

where f is the frequency in GHz, θ is the angle of elevation, and g is the antenna averaging factor that depends mainly on the frequency and antenna parameters. σ_0 can be obtained in dB from the wet term of radio refractivity N_{wet} which, in turn, depends on the value of temperature T and H_R [29]. Consider

$$\begin{aligned} \sigma_0 &= 0.0036 + N_{\mathrm{wet}} \times 10^{-4}, \\ N_{\mathrm{wet}} &= 3732 \times \frac{H_R e_S}{T^2}, \end{aligned} \tag{11}$$

where e_S is the temperature-dependent saturation vapor pressure that can be calculated from [29]. The mean value of H_R measured by MMD is 82.375%. With σ_S, the tropospheric scintillation fade depth A_{scint} is estimated using the ITU model [23] for different probabilities of occurrence (P).

The power spectral density (PSD) of the fading is time variant and can be approximated by low-pass filter (LPF) [28]. The LPF in [28] is used, and the resultant signal is then uniformly distributed and combined with A_{scint} to obtain the estimated signal series of tropospheric scintillation.

4.4. Complementary Blocks and Quality Indicator. The total performance of the correlated impairments is a combination of the LMS multistate mobility and tropospheric scintillation models as declared in (2). However, as the signal passes through the channel, several other constraints cause additional losses, such as system loss and free space loss (FSL). The latter depends on the transmitted frequency and the distance difference between the satellite and the mobile terminal as revealed in (12). Consider

$$\mathrm{FSL} = 20 \log\left(\frac{4\pi d}{\lambda}\right). \tag{12}$$

Consequently, the estimation of the received SNR, which is the received signal power P_r to noise [$P_n = 10\log(k_B\mathrm{TBW})$] ratio is included in the design. Equation (13) [30, 31] is utilized to estimate the received power P_r in dBW. Consider

$$P_r = \mathrm{EIRP} + G_r - \mathrm{FSL} - L_S - L_{\mathrm{LMS}}, \tag{13}$$

where EIRP is the effective isotropic radiated power in dBW that depends on the transmitted power and the transmitter antenna gain; G_r is the receiver gain; L_S is the total system loss; and L_{LMS} is the total LMS channel loss that has not been considered in previous studies, which represents the total fading losses that can be obtained from the ELMSC model. After the insertion of the channel fading effect to the transmitted signal, additive white Gaussian noise (AWGN) is added.

The atmospheric impairments have a negative effect on the data after being demodulated in the receiver. The effect appears, for example, as a decrease in E_b/N_o or packet error

rate. These ratios can be utilized to generate the proposed indexing for optimal physical or link layer adaptations for the current instantaneous transmission time interval (TTI). Equation (14) is used to obtain E_b/N_o (in dB) for widely used modulation schemes and code rates (MODCOD) in satellite communications. Consider

$$\frac{E_b}{N_o} = \frac{E_S}{N_o} - 10\log(K), \tag{14}$$

$$\frac{E_S}{N_o} = \text{SNR} + 10\log\left(\frac{\text{BW}}{R}\right), \tag{15}$$

where $K = \log_2(M) \times R_C$, M is the modulation order, R_C is the code rate, E_s/N_o is the symbol energy to noise ratio, BW is the bandwidth, and R is the symbol rate. For fixed R and BW, E_b/N_o is directly proportional to SNR and inversely proportional to M and R_C. Therefore, after substituting ((12)–(14)) to (15), the estimated E_b/N_o is obtained as shown in (16). Consider

$$\frac{E_b}{N_o} = \text{EIRP} + \frac{G}{T} - 20\log\left(\frac{4\pi d}{\lambda}\right) - L_{\text{LMS}} - L_S - k_B + 10\log\left(\frac{K}{R}\right), \tag{16}$$

where G/T is the figure of merit of the receiver antenna and k_B is the Boltzmann constant. E_b/N_o is used as a quality indicator for the ELMSC model.

5. Results and Discussion

For realistic channel estimation, the estimation was based on the actual measurements of signal performance under dynamic weather conditions. The model design results are organized based on the arrangements of the blocks in Figure 4.

The generated signal (Figure 5(a)) exhibits rapid variation at a transmission frequency of 11.6 GHz. Figure 5(b) shows that the distribution of the resultant signal did not change after filtering.

The state series shown in Figure 5(c) comprises the three states distributed randomly with respect to the probability of occurrence of each state. Figure 6 provides a zoomed in version of Figure 5 to recognize the generated samples clearly. The succeeding results are presented based on the zoomed in version to identify clearly the effect of each block in the ELMSC model. For accurate comparison with other models and better modeled signal resolution, the comparison was based on extended samples as in Figure 5.

The resultant multipath signal passes through the multi-state model with respect to the state series. If the current state is 1, then the multipath signal samples will pass through the clear LOS model, which is composed of three stages. First, the samples are multiplied by σ_{LOS} to obtain the Rician multipath signal. Second, the direct signal component (a) is added. Lastly, I_S is added at different speeds. The resultant clear LOS fading is shown in Figure 7.

The direct signal component (a) is calculated based on (1), where Rice factor $K = 11.5$ dB. The value of K is assumed based on the measurements discussed in Section 3. The channel parameters are listed in Table 4.

During the measurement campaign, vehicle speed was recorded simultaneously with the measurement data to account for the additional losses from the movement of the satellite terminal at different speeds. These losses are mainly due to the pointing misalignment caused by the antenna

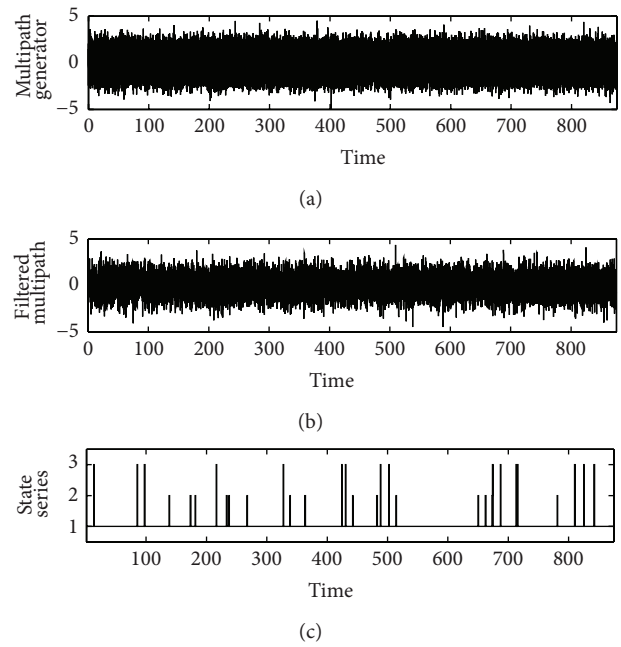

Figure 5: Multipath generated signal and state series: (a) generated samples, (b) filtered signal, and (c) state series.

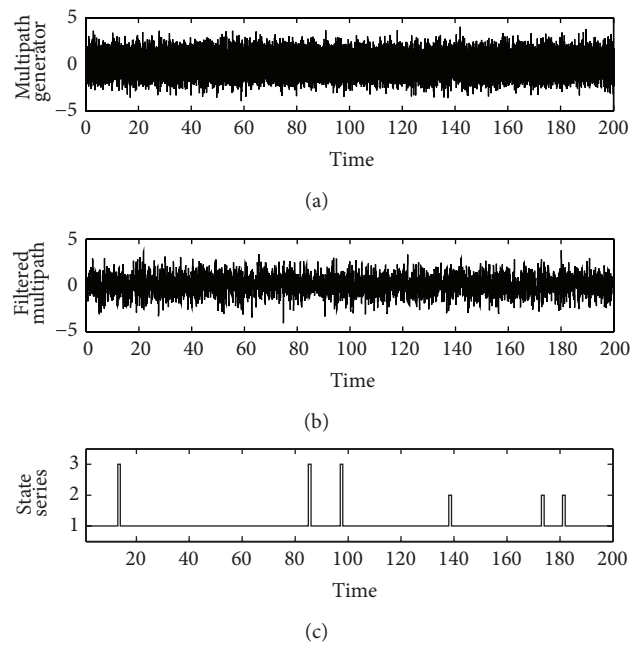

Figure 6: Zoomed in version of the generated signal and state series: (a) generated samples, (b) filtered signal, and (c) state series.

Table 4: Models' parameters.

Parameter	ELMSC	Conventional [1]
Satellite orbit	GEO	GEO
Frequency band	Ku	Ku
Rice K factor	11.5 dB	17 dB
Climatic area	Temperate-tropical	Temperate
Antenna type	Directional antenna	Directional antenna

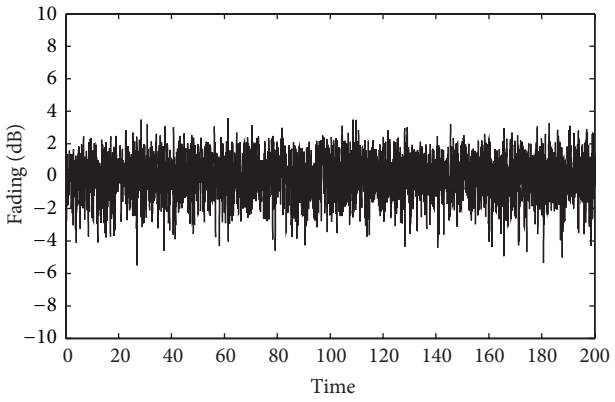

Figure 7: Fading in the clear LOS state.

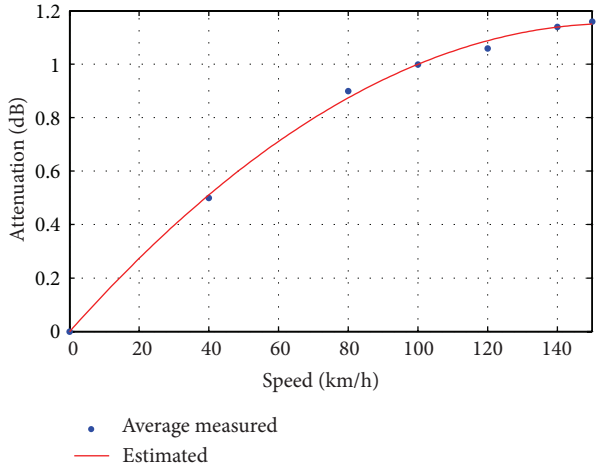

Figure 8: Signal losses with respect to satellite terminal speed.

tracking error. The resultant average measurement data of signal attenuation with respect to satellite terminal speed is shown in Figure 8.

With respect to terminal speed, the average values of several measured signal samples have been obtained. The speed of approximately 40, 80, 100, 120, 140, and 150 km/h has been considered in the measurement campaign as well as the stationary (zero speed) case. The measurements show that the signal is further attenuated by 0.6 dB when the terminal moves at 60 km/h. The attenuation slope changes when the speed reaches 80 km/h. The attenuation level increases more slightly than when speed is below 80 km/h. The losses reach approximately 1 dB at 100 Km/h, 1.15 dB at 140 Km/h, and 1.18 dB at 150 Km/h. However, as discussed in Section 4.2 and expressed in Figure 8, the proposed equation (9) provides an accurate estimation of signal performance at different terminal speeds with RMSE equal to 0.02407. To the best of our knowledge, this model is the first to be designed for the estimation of LMS channel impairments at different terminal speeds based on measurement data at the Ku-band.

Based on the experimental measurements in the clear LOS scenario, the signal model at state 1 provides less RMSE estimation than the conventional model proposed earlier. This finding can be clearly proven by comparing the CDF and PDF of the measured SNR and the conventional model with the proposed model. After adding the effect of FSL from (12) to obtain the channel fade and AWGN to the transmitted signal carrier, the CDF and PDF of the estimated received power were obtained as shown in Figure 9.

To identify the effect of the proposed multistate part of the ELMSC model with respect to the clear LOS measured signal and conventional model, Figure 9 shows the CDF and PDF of the received SNR prior to the addition of the proposed tropospheric scintillation model. The effect of the proposed I_S module appeared as a change in the slope difference of CDF as shown in Figure 9(a). This leads to a decrease in the RMSE of the proposed model, whereas the change in the K factor shifted the CDF for few dBs towards the measured value, which approaches the CDF slope of the measured SNR compared with the conventional model. Until this point, the PDF performance of the proposed model exhibits a significant enhancement compared with the conventional model such that it approaches the PDF of the measured SNR and will be further enhanced if tropospheric scintillation is included.

In the case of state 2, the shadowing model is applied to the generated multipath signal in Figure 5(b). The model is a combination of two distributions. The slow variation trail is composed of three stages before the addition of rapid variation. Finally, the signal passes through the proposed I_S block as discussed in Section 4.2. The effect of these steps is shown in Figure 10.

The slow variation trail begins with the generation of random normal distribution samples. One of the objectives of the experimental measurements is to measure the average power absorption for each scenario. 13 dB mean value is used as proposed in [32].

The distribution is then converted to a log-normal distribution before rate conversion and interpolation as discussed in Section 4.2 and shown in Figure 10(a). Figure 10(b) shows that the signal variation performance does not change after this step, except for the higher number of samples that accounts for the generated rapid variations. Figure 10(c) shows the simulated shadowing fade.

The signal level in a full blocking environment (state 3) usually reaches the noise floor level, as discussed in Section 4.2, with multipath fluctuations of specific standard deviation σ_{BL} that is typically greater than σ_{LOS} [13]. Therefore, the resultant signal from the multipath generator is multiplied by the value of σ_{BL}, which is assumed according to

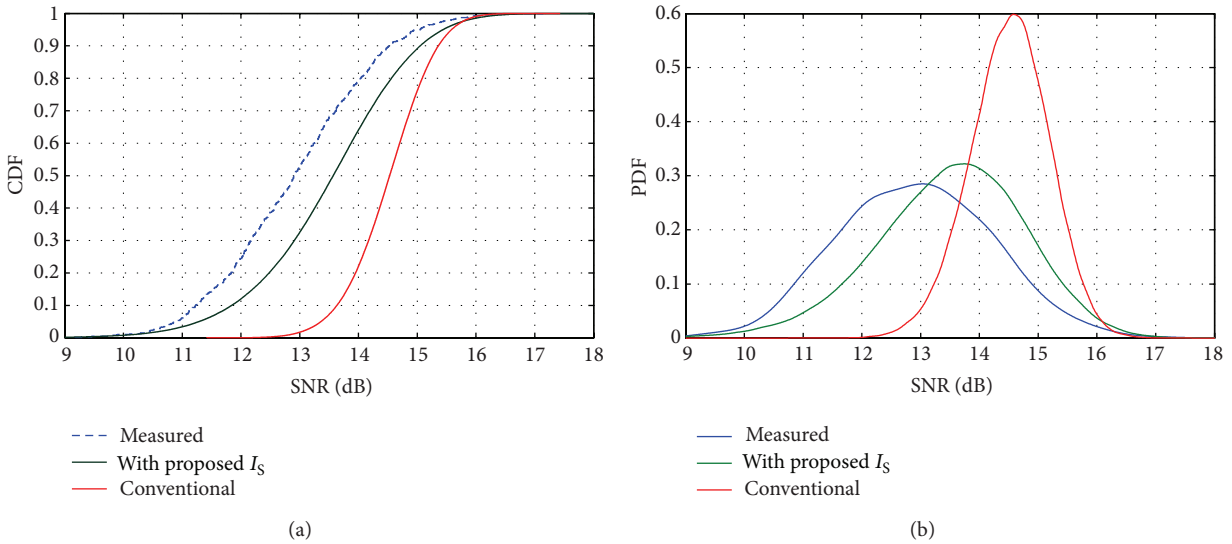

Figure 9: Received SNR in clear LOS state: (a) CDF and (b) PDF.

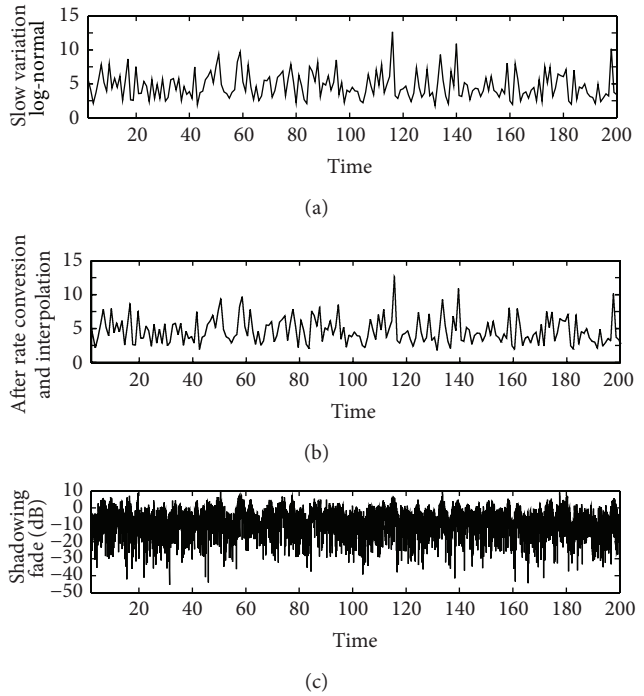

Figure 10: Simulated fade attributed to shadowing: (a) the generated slow variation lognormal distribution, (b) signal after rate conversion and interpolation, and (c) the aggregated fade.

[1]. However, the simulated signal of the multistate model is a result of the switching process of the three aforementioned states. Switching control is based on the state series generated (shown in Figure 5(c)).

Another remarkable impairment to the LMS channel is tropospheric scintillation which gives rise to signal turbulence because of the rapid change in the refractive index of the medium. The change in the refractive index of the medium is because of the water particles in the troposphere. Therefore, the H_R percentage has a vital role in the signal performance and standard deviation of fluctuations.

H_R is varied from one region to another according to their different weather parameters. Therefore, two different signals were modeled each with its specific region, one with lower standard deviation of fluctuation as proposed by [28] represents a temperate region and the other proposed in this study for higher humidity regions as in tropics based on the measured H_R discussed in Section 4.3. Figure 11 shows the

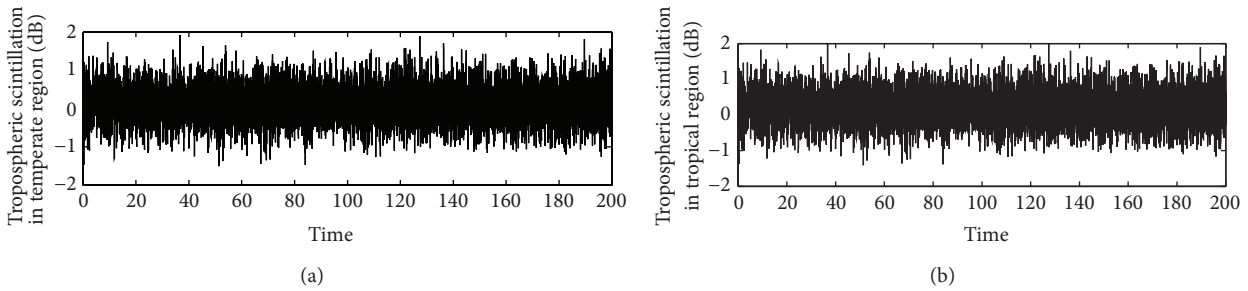

Figure 11: Modeled fluctuations caused by tropospheric scintillation: (a) temperate region and (b) tropical region LMS link scenarios.

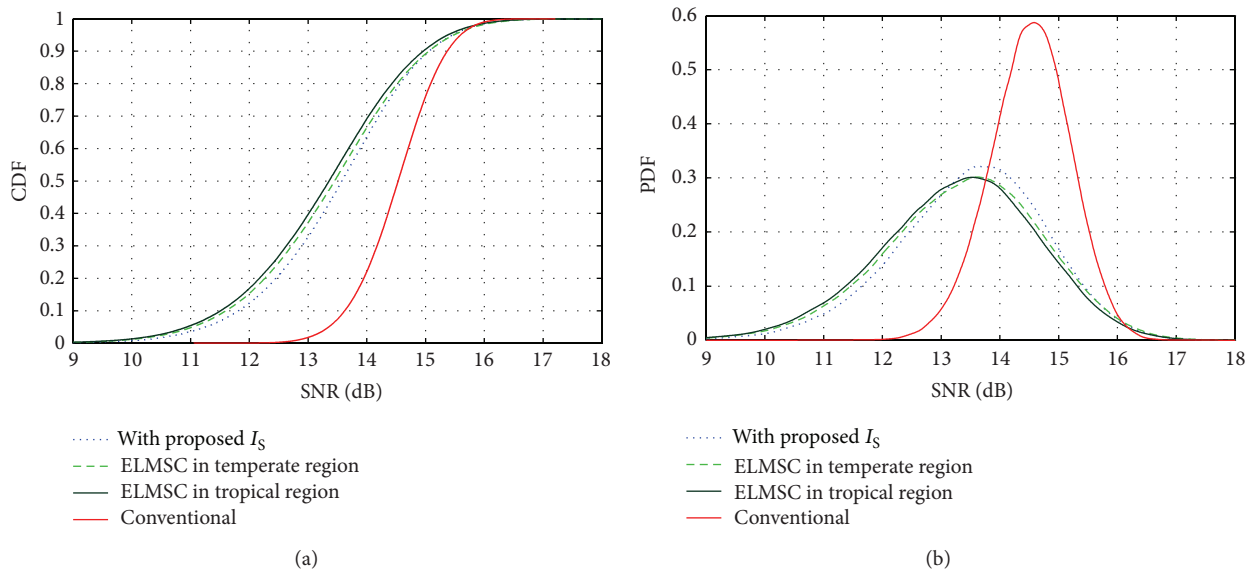

Figure 12: Tropospheric scintillation effect: (a) CDF and (b) PDF.

estimated tropospheric scintillation performance according to the proposed model.

Figure 11 shows the difference in the estimated signal samples between temperate and tropical regions. To identify the effect of tropospheric scintillation clearly in both regions, Figure 12 shows the CDF and PDF of the received SNR in temperate and tropical regions for clear LOS state after adding the tropospheric scintillation effect.

It is shown in Figure 12 that the distribution of the samples in tropical regions is different from the temperate regions according to its weather parameters especially the higher relative humidity and hence higher water particles which cause extra fluctuations compared with the temperate regions. Therefore, the fluctuation performance reflects a change in CDF and PDF with respect to the original distribution functions when tropospheric scintillation is excluded. It can be noticed that the peak value of the PDF of the estimated SNR in tropical region is moved to lower SNR because of the different weather parameters and approaches the peak value of the measured SNR (as seen later in Figure 14). As discussed in Section 2.4, fade depth depends on the probability of exceedance time (P). Figure 13 shows the tropospheric scintillation effect for several fade depths at different P.

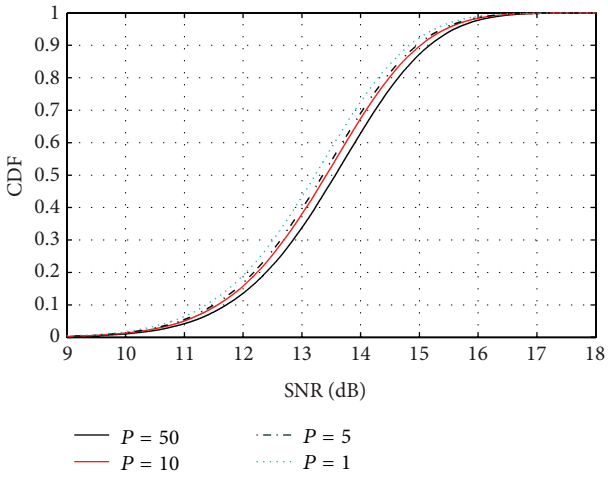

Figure 13: Tropospheric scintillation effect at different P.

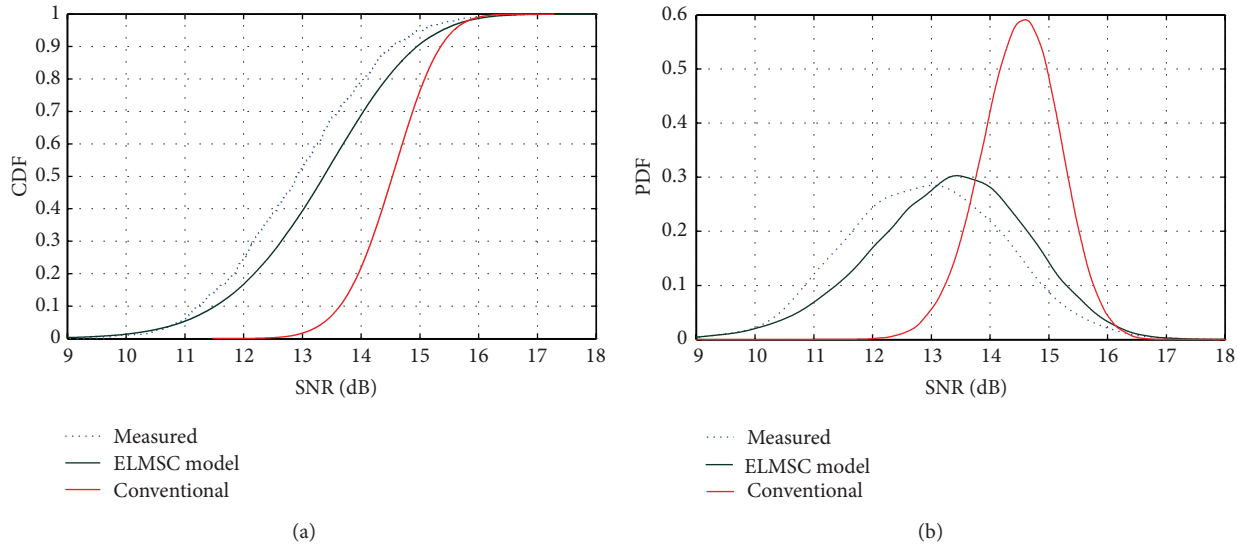

Figure 14: Comparison of channel models with the measured SNR: (a) CDF and (b) PDF.

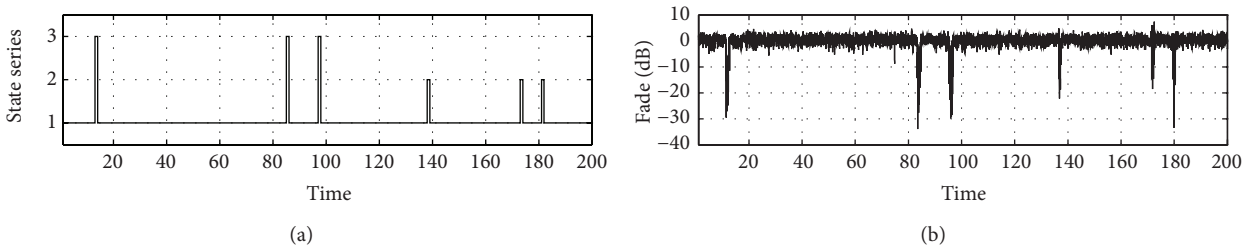

Figure 15: Signal performance of the ELMSC model: (a) state series and (b) signal fade.

The probability of exceedance time significantly affects the distribution function. P is directly proportional to fade depth; the highest level reached $P \geq 1$.

The effect of P was predicted based on the experimental measurements obtained by ITU [23]. The proposed ELMSC model at tropical regions in clear LOS is compared with the measurement data (discussed in Section 3) and the conventional model used, as shown in Figure 14.

The CDF and PDF show that the ELMSC model provides less RMSE regarding the estimation of the channel compared with the conventional model. The PDF of the proposed model reached a peak value of approximately 0.3 among 8 dBs. This value approaches the measured value (difference = 0.02). By contrast, the conventional model reached the peak value of approximately 0.59 among 5 dBs, which significantly differs from the measured value (difference = 0.31). Table 5 shows the RMSE and the differences in variance and PDF's peak values of the ELMC and conventional model compared with the measured time series signal. The proposed fade for three states is shown in Figure 15.

The variance in fluctuation during state 1 is equal to 1.8133, which approaches the measured value of 1.6408 and is closer than the value of conventional variance (0.4508). The minimum duration for one state is set to four times the sampling period to reflect the real-world environment, such that, when the mobile terminal passes under trees, it usually stays in this environment for more than one sample period.

Table 5: Comparison with the measured data.

Parameter	ELMSC	Conventional [1]
RMSE	0.0262	0.1268
PDF's peak value difference	0.02	0.31
Variance difference	0.1725	1.3625

The quality indicator included in the model is used to identify the channel quality in several widely used modulation schemes and code rates (MODCODs) that are used in video broadcasting protocols such as digital video broadcasting via satellite-second generation (DVB-S2) [33]. Figure 16 shows the mean E_b/N_o value for the three states. These values were estimated at the input of the decoder.

E_b/N_o is used as a quality indicator for the ELMSC model. The value is examined at different MODCODs. E_b/N_o determines the availability of the received signal as well as its quality. Availability is determined based on the value of a quality indicator. Therefore, to achieve signal availability for systems that use, for example, a minimum E_b/N_o value of 4 dB, the signal is available in the clear LOS scenario at all times. In the shadowing scenario, the signal is available

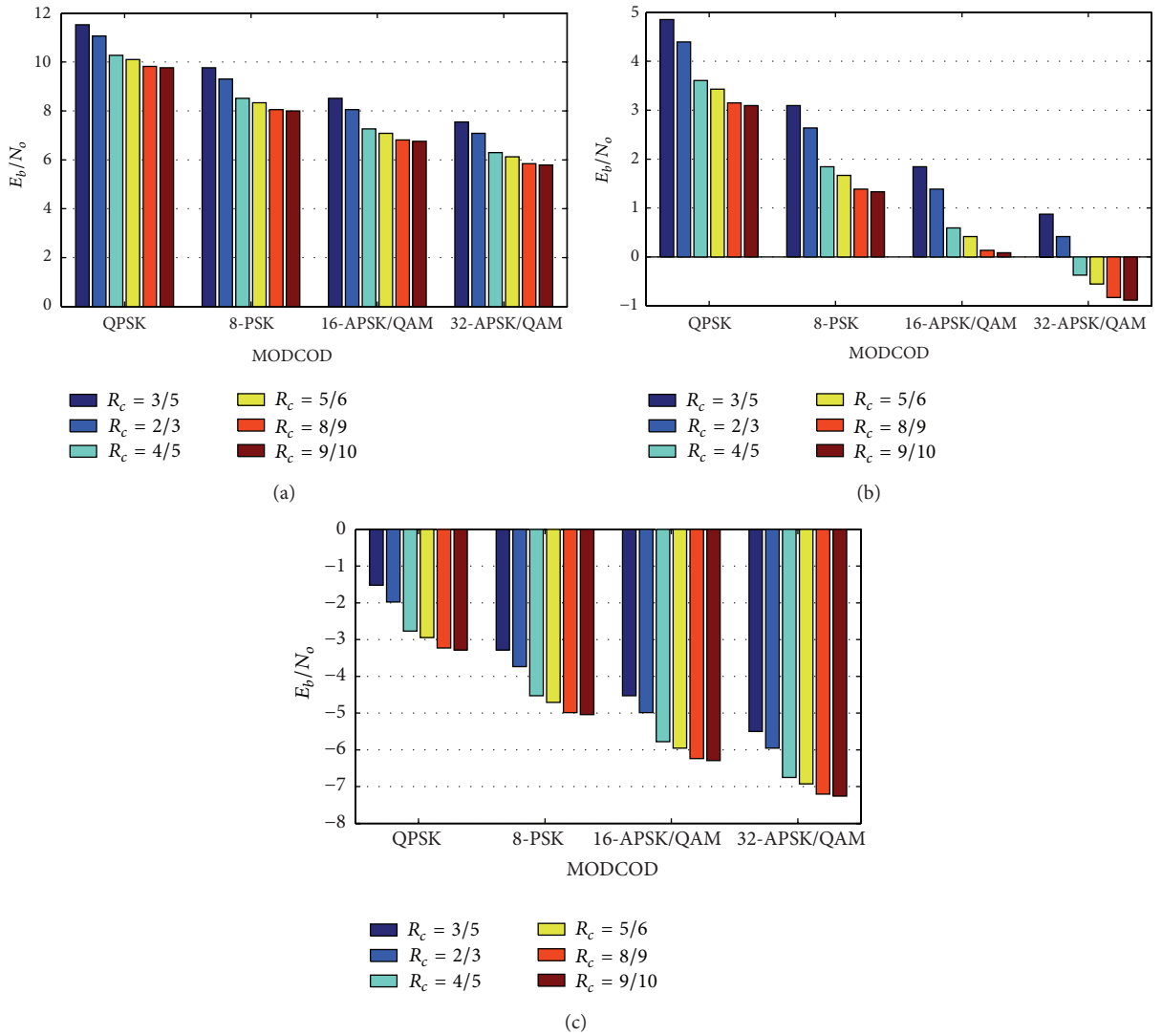

FIGURE 16: E_b/N_o (in dB) at different MODCODs: (a) clear LOS, (b) shadowing, and (c) blockage scenarios.

when QPSK at $R_C = 3/5$ and 2/3 only, whereas no signal is available in the blockage state. Moreover, the values of E_b/N_o at different MODCODs and environments can determine the error rates in the data received. Therefore, the quality indicator is essential in the design of the channel model to specify the availability and error rates for the signal under different channel conditions and system parameters.

6. Conclusion

A model for LMS channel modeling at the Ku-band was presented in this study based on experimental measurements. The design considers the three typical channel states, namely, clear LOS, shadowing, and blockage states. The proposed model has new features and was proven to be comprehensive, reliable, and less RMSE than conventional model. The channel states were modeled and combined with the new module to account for the satellite tracking error attributed to the dynamic terminal speeds. The tropospheric scintillation impairments were presented and modeled for the LMS scenario at temperate and tropical regions. Finally, a quality indicator module was presented and included in the proposed ELMSC model. The measurement data were provided, and the time series synthesizer, PDF, and CDF of the proposed model were presented and compared with the conventional model. A fairly good agreement was observed between the proposed ELMSC model outputs and the measurements. The model can be applied to temperate and tropical regions for narrow- and wide-band signals at various modulation and coding schemes and different satellite terminal speeds. The model and its associated modules can be used to study the signal performance, availability, and error rates of different services, including communications, broadcast, and navigation, as well as to develop fade mitigation techniques for channel-aware strategies.

Conflict of Interests

The authors declare that there is no conflict of interests regarding the publication of this paper.

Acknowledgment

The support provided by the Ministry of Higher Education in Malaysia through project grant code ERGS/1-2012/5527096 is duly acknowledged.

References

[1] S. Scalise, H. Ernst, and G. Harles, "Measurement and modeling of the land mobile satellite channel at Ku-band," *IEEE Transactions on Vehicular Technology*, vol. 57, no. 2, pp. 693–703, 2008.

[2] F. P. Fontán, M. Vázquez-Castro, C. E. Cabado, J. P. García, and E. Kubista, "Statistical modeling of the LMS channel," *IEEE Transactions on Vehicular Technology*, vol. 50, no. 6, pp. 1549–1567, 2001.

[3] A. M. Al-Saegh, A. Sali, J. S. Mandeep, and A. Ismail, "Extracted atmospheric impairments on earth-sky signal quality in tropical regions at Ku-band," *Journal of Atmospheric and Solar-Terrestrial Physics*, vol. 104, pp. 96–105, 2013.

[4] J. S. Mandeep and Y. Y. Ng, "Satellite beacon experiment for studying atmospheric dynamics," *Journal of Infrared, Millimeter, and Terahertz Waves*, vol. 31, no. 8, pp. 988–994, 2010.

[5] C. Loo and N. Secord, "Computer models for fading channels with applications to digital transmission," *IEEE Transactions on Vehicular Technology*, vol. 40, no. 4, pp. 700–707, 1991.

[6] G. E. Corazza and F. Vatalaro, "Statistical model for land mobile satellite channels and its application to nongeostationary orbit systems," *IEEE Transactions on Vehicular Technology*, vol. 43, no. 3, pp. 738–742, 1994.

[7] M. Pätzold, U. Killat, and F. Laue, "An extended suzuki model for land mobile satellite channels and its statistical properties," *IEEE Transactions on Vehicular Technology*, vol. 47, no. 2, pp. 617–630, 1998.

[8] E. Lutz, D. Cygan, M. Dippold, F. Dolainsky, and W. Papke, "The land mobile satellite communication channel—recording, statistics, and channel model," *IEEE Transactions on Vehicular Technology*, vol. 40, no. 2, pp. 375–386, 1991.

[9] K. P. Liolis, A. D. Panagopoulos, and S. Scalise, "On the combination of tropospheric and local environment propagation effects for mobile satellite systems above 10 GHz," *IEEE Transactions on Vehicular Technology*, vol. 59, no. 3, pp. 1109–1120, 2010.

[10] D. Rey Iglesias and M. G. Sanchez, "Semi-Markov model for low-elevation satellite-earth radio propagation channel," *IEEE Transactions on Antennas and Propagation*, vol. 60, no. 5, pp. 2481–2490, 2012.

[11] A. D. Panagopoulos, P. D. M. Arapoglou, and P. G. Cottis, "Satellite communications at KU, KA, and V bands: propagation impairments and mitigation techniques," *IEEE Communications Surveys & Tutorials*, vol. 6, no. 3, pp. 2–14, 2004.

[12] S. Scalise, R. Mura, and V. Mignone, "Air interfaces for satellite based digital TV broadcasting in the railway environment," *IEEE Transactions on Broadcasting*, vol. 52, no. 2, pp. 158–166, 2006.

[13] F. P. Fontan, A. Mayo, D. Matote et al., "Review of generative models for the narrowband land mobile satellite propagation channel," *International Journal of Satellite Communications and Networking*, vol. 26, no. 4, pp. 291–316, 2008.

[14] A. Vanelli-Coralli, G. E. Corazza, G. K. Karagiannidis et al., "Satellite communications: research trends and open issues," in *Proceedings of the International Workshop on Satellite and Space Communication (IWSSC '07)*, pp. 71–75, September 2007.

[15] Z. K. Adeyemo, O. O. Ajayi, and F. K. Ojo, "Simulation model for a frequency-selective land mobile satellite communication channel," *Innovative Systems Design and Engineering*, vol. 3, pp. 71–84, 2012.

[16] M. Milojević, M. Haardt, E. Eberlein, and A. Heuberger, "Channel modeling for multiple satellite broadcasting systems," *IEEE Transactions on Broadcasting*, vol. 55, no. 4, pp. 705–718, 2009.

[17] A. Abdi, W. C. Lau, M. Alouini, and M. Kaveh, "A new simple model for land mobile satellite channels: first- and second-order statistics," *IEEE Transactions on Wireless Communications*, vol. 2, no. 3, pp. 519–528, 2003.

[18] D. Arndt, A. Ihlow, T. Heyn, A. Heuberger, R. Prieto-Cerdeira, and E. Eberlein, "State modelling of the land mobile propagation channel for dual-satellite systems," *EURASIP Journal on Wireless Communications and Networking*, vol. 2012, pp. 1–21, 2012.

[19] A. Mehmood and A. Mohammed, "Characterisation and channel modelling for satellite communication systems," in *Satellite Communications*, N. Diodato, Ed., pp. 133–152, InTech, Rijeka, Croatia, 2010.

[20] ITU, *Propagation Data Required for the Design of Earth-Space Land Mobile Telecommunication Systems*, International Telecommunication Union—Recommandation, 2009.

[21] A. Adhikari and A. Maitra, "Studies on the inter-relation of Ku-band scintillations and rain attenuation over an Earth-space path on the basis of their static and dynamic spectral analysis," *Journal of Atmospheric and Solar-Terrestrial Physics*, vol. 73, no. 4, pp. 516–527, 2011.

[22] A. Adhikari, A. Bhattacharya, and A. Maitra, "Rain-induced scintillations and attenuation of ku-band satellite signals at a tropical location," *IEEE Geoscience and Remote Sensing Letters*, vol. 9, no. 4, pp. 700–704, 2012.

[23] ITU, "Propagation data and prediction methods required for the design of Earth-space telecommunication systems," Tech. Rep. P.618-11, International Telecommunication Union—Recommandation, 2013.

[24] P. Burzigotti, R. Prieto-Cerdeira, A. Bolea-Alamañac, F. Perez-Fontan, and I. Sanchez-Lago, "DVB-SH analysis using a multi-state land mobile satellite channel model," in *Proceeding of the 4th Advanced Satellite Mobile Systems (ASMS '08)*, pp. 149–155, Bologna, Italy, August 2008.

[25] F. Pérez Fontán and P. Mariño Espiñeira, "Multipath: narrowband channel," in *Modeling the Wireless Propagation Channel*, chapter 5, pp. 105–135, John Wiley & Sons, 2008.

[26] R. Prieto-Cerdeira, F. Perez-Fontan, P. Burzigotti, A. Bolea-Alamaac, and I. Sanchez-Lago, "Versatile two-state land mobile satellite channel model with first application to DVB-SH analysis," *International Journal of Satellite Communications and Networking*, vol. 28, no. 5-6, pp. 291–315, 2010.

[27] F. Pérez Fontán and P. Mariño Espiñeira, "The land mobile satellite channel," in *Modeling the Wireless Propagation Channel*, chapter 9, pp. 213–227, John Wiley & Sons, New York, NY, USA, 2008.

[28] S. Cioni, R. de Gaudenzi, and R. Rinaldo, "Channel estimation and physical layer adaptation techniques for satellite networks

exploiting adaptive coding and modulation," *International Journal of Satellite Communications and Networking*, vol. 26, no. 2, pp. 157–188, 2008.

[29] ITU, "The radio refractive index: its formula and refractivity data," in *International Telecommunication Union—Recommandation*, pp. 453–510, 2012.

[30] L. J. Ippolito, *Satellite Communications Systems Engineering: Atmospheric Effects, Satellite Link Design and System Performance* , Wiley, New York, NY, USA, 2008.

[31] V. K. Sakarellos, D. Skraparlis, A. D. Panagopoulos, and J. D. Kanellopoulos, "Outage performance analysis of a dual-hop radio relay system operating at frequencies above 10 GHz," *IEEE Transactions on Communications*, vol. 58, no. 11, pp. 3104–3109, 2010.

[32] F. Pérez Fontán and P. Mariño Espiñeira, "Shadowing and multipath," in *Modeling the Wireless Propagation Channel*, chapter 6, pp. 137–151, John Wiley & Sons, New York, NY, USA, 2008.

[33] ETSI, "Digital Video Broadcasting (DVB) ; second generation framing structure, channel coding and modulation systems for broadcasting interactive services, news gathering and other broadband satellite applications (DVB-S2)," Tech. Rep. EN 302 307 V1.3.1, ETSI, 2013.